Journal of Materials Chemistry A

ROYAL SOCIETY OF CHEMISTRY

REVIEW

View Article Online
View Journal | View Issue

Cite this: J. Mater. Chem. A, 2023, 11, 3245

Recent advances in metal-free covalent organic frameworks for photocatalytic applications in energy and environmental fields

Zilong Zhou,[a] Yuting Xiao, *[a] Jing Tian,[a] Ning Nan,[a] Renjie Song *[a] and Jinheng Li *[bc]

Received 9th December 2022
Accepted 9th January 2023

DOI: 10.1039/d2ta09582c

rsc.li/materials-a

Covalent organic frameworks (COFs) are an emerging class of multivacancy organic polymers with a large specific surface area, stable pore size, high crystallinity, and good stability. Moreover, the tailorability of the structure provides a theoretical basis for the preparation of various COF-based materials. However, many COFs rely on metal ions to enhance their photocatalytic performance. Therefore, considering environmental factors and the necessity for developing COF applications, an in-depth review on metal-free COF photocatalysts from an environmental perspective is urgently needed. This review provides a comprehensive overview of the synthesis strategy of COFs, and the applications of metal-free COFs as photocatalysts in environmental fields, including water splitting, CO_2 reduction, pollutant degradation, organic synthesis and environmental remediation. Otherwise, the review summarizes the current and future development of the field and provides perspectives on trends for future challenges and outlooks.

Introduction

Energy shortages and environmental pollution due to the massive consumption of fossil fuels have become serious concerns for human society. In this regard, low-cost and environmentally friendly photocatalytic technologies have provided new hope for overcoming the current energy and environmental crises.[1–3] However, traditional photocatalysts generally suffer from limited solar energy utilisation efficiency[4] and low photogenerated carrier separation efficiency.[5] In addition, the catalytic mechanism is not well understood. Therefore, the development of new visible-light-responsive photocatalysts and the elucidation of their structures are key research areas for realising efficient and stable light-driven photocatalysts for environmental remediation and energy conversion applications.

Conventional homogeneous photocatalysts exhibit excellent catalytic performance,[6] which has led to their widespread industrial use. However, they are difficult to separate from the products or reaction medium after the reaction.[7] Additionally, precious metal photocatalysts are prone to environmental pollution, difficult to recycle, and not conducive to product purification. Therefore, various non-homogeneous photocatalysts and inorganic porous materials have emerged, including zeolites,[8] silica heterojunctions,[9] and metal–organic frameworks (MOFs).[10] However, inorganic porous materials have active site uncertainty and MOFs have poor stability.[11] A large number of these photocatalysts are also heavily dependent on precious metals to enhance their performance, and a large number of metal ions remain in the material, seriously affecting their application. Since Yaghi introduced the first covalent organic framework (COF) in 2005,[12] the preparation of COFs has attracted significant research interest. COFs have shown great potential for application in gas separation and storage,[13] adsorption of metal ions,[14] sensors,[15,16] optoelectronic devices,[17,18] and heterogeneous catalysis.[19,20] In particular, COF-based electrocatalysts have achieved considerable advances in the water cycle,[21–23] the carbon energy cycle,[24–26] and supercapacitors;[27,28] the developments of these energy storage and conversion applications have been discussed in detail in some very excellent review articles.[29,30]

Since the discovery of heterogeneous photocatalysis over semiconducting COFs by Jiang and co-workers,[31] COF-based materials have been widely used in diverse photocatalytic fields, such as water splitting,[32,33] CO_2 reduction,[34,35] organic synthesis[36,37] and environmental remediation.[38–40] COF-based photocatalysts have several advantages compared to other inorganic photocatalysts: (i) the defined structure–property relationship in COFs is favourable for modification; (ii) COFs have higher specific surface areas, resulting in hundreds or even thousands of active sites; (iii) COFs have good crystallinity, which ensures their stability and significantly reduces the

[a]Key Laboratory of Jiangxi Province for Persistent Pollutants Control and Resources Recycle, Nanchang Hangkong University, Nanchang 330063, China. E-mail: srj0731@hnu.edu.cn; yutingxiao9@sina.com

[b]School of Chemistry and Chemical Engineering, Henan Normal University, Xinxiang, Henan 475004, China. E-mail: jhli@hnu.edu.cn

[c]State Key Laboratory of Applied Organic Chemistry, Lanzhou University, Lanzhou 730000, China

electron–hole recombination frequency; (iv) the periodically ordered columnar array of the π–π-conjugated system facilitates electron delocalisation and endows COFs with excellent electron transport properties and photoconductivity; and (v) the designability of the donor–acceptor structure and introduction of suitable building blocks facilitate electron–hole separation and enhance the photocatalytic performance of COFs.[41–45]

Most COFs rely on loaded metals, such as Pt, Ir, and Re, to enhance their photocatalytic activity.[46–48] Therefore, considering environmental factors and the necessity for developing COF applications, an in-depth review on metal-free COF photocatalysts from an environmental perspective is urgently needed. This review provides a detailed introduction to the main building blocks of COFs and their application as photocatalysts. Subsequently, the current and future development of metal-free COF-based photocatalysts is summarised and discussed.

Design and synthesis of COF-based photocatalysts

Building blocks

Similar to inorganic semiconductor photocatalysts, organic photocatalysts operate by the absorption of photons, resulting in intramolecular electron transfer from the highest occupied molecular orbital (HOMO) to the lowest unoccupied molecular orbital (LUMO). The HOMO and LUMO correspond to the valence and conduction bands in inorganic semiconductor materials, respectively. COF-based photocatalysts use different organic building blocks, such as triazines, porphyrins, and pyrenes, as electron donors or acceptors. Additionally, reactive sites, which are usually symmetrically distributed, are appropriately introduced into these units to determine the active sites of the synthesised material and guide the orderly arrangement of units. These units are then connected by covalent bonds formed by reversible reactions to produce crystalline materials with regularly arranged polygonal pore structures, where the periodically arranged pore walls provide abundant active sites. Therefore, COFs with different photocatalytic properties can be easily obtained by the flexible selection of building blocks.

Triazine rings, which are the light-harvesting centres in graphitic carbon nitride (g-C_3N_4), have an excellent photocatalytic structure and are widely used as COF building blocks. g-C_3N_4 has long been of interest as a photocatalytic material,[49] however, its slow carrier migration kinetics and rapid electron–hole recombination rate limit its application. Nevertheless, triazine rings can effectively modulate the energy band structure of COFs to reduce the band gap and enhance the light-harvesting ability.[50] Additionally, the ordered donor–acceptor structure of COFs improves the efficiency of photoinduced electron transfer and charge separation. Therefore, COFs exhibit significantly better photocatalytic activity than monolithic g-C_3N_4. In 2020, the synthesis of an all-sp^2 carbon two-dimensional (2D) COF was achieved by the introduction of triazine. The prepared COF was a photosensitive semiconductor with an optical band gap of 2.46 eV and excellent carrier conductivity. It exhibited excellent performance and reusability for the photocatalytic degradation of dyes and C–H functionalisation of aromatic and heteroaromatic hydrocarbons.[51]

Porphyrins are widely found in nature, where they play a crucial role in photosynthesis and enzymatic reactions. Porphyrins and porphyrin-like compounds exhibit excellent coordination capabilities and unique photophysical and electronic properties. Therefore, porphyrin structures are commonly used as building blocks in COFs. Verduzco *et al.*[52] reported the development of two porphyrin-based COFs with a wide light absorption range. The prepared COFs exhibited excellent photocatalytic activity for the polymerisation of various monomers under different light and solvent conditions. Porphyrin-based 2D-COFs and highly active flexible membranes have also been reported, which show excellent photocatalytic performance. For example, porphyrin-based 2D-COF photocatalysts can facilitate the photoinduced activation of C–H bonds between the *p*-positions of substituted aryl diazonium salts and heteroaromatics with high selectivity (~99%) and high yields.[53]

Pyrene is another widely used building block for preparing strong conjugated structures in COFs. In 2021, Beyzavi[54] reported the synthesis of a new COF based on imine bonds from pyrene, with an interesting double-porous structure and good crystallinity. The prepared COF was a recyclable non-homogeneous photocatalyst with excellent catalytic effects for the decarboxylative difluoroalkylation and oxidative cyclisation reactions. In 2022, Huo *et al.*[55] reported a new COF with 1,3,6,8-tetra(*p*-formylphenyl)pyrene as the structural unit, which showed excellent photocatalytic activity for the hydroxylation of aryl boronic acids.

Connection keys

The modular structural dynamics of the reversible covalent bonds in COFs are crucial for obtaining crystallinity. As shown in Fig. 1, the reported linkages for constructing COFs include boronate ester, imine, hydrazone, and alkene bonds.

Boronate ester/boroxine ring linkages. The first COF was synthesised by Yaghi *et al.*[12] in 2005. It was produced by the self-condensation of boronic acid and the dehydration–condensation of boronic acid hydroxyl groups, and contained boroxine ring and boronate ester linkages. The highly reversible self-condensation and dehydration–condensation reactions guided the ordered joining of material units and imparted excellent crystallinity to the material. However, COFs with these linkages have poor stability and hydrolyse easily in H_2O, which limits their application. Nevertheless, COFs with these linkages were heavily explored in the early development of COF materials.

Amine bonding. COFs with amine linkages are constructed by acid-catalysed Schiff base aldehyde–amine condensation reactions. Compared to boronate ester- and boroxine ring-linked bonds, imine-bonded COFs have superior stability. However, owing to the weak reversibility of the Schiff base reaction, the crystallinity of subamine-bonded materials is typically lower than that of boronate ester- or boroxine ring-linked materials. In 2009, Yaghi *et al.*[56] reported the first example of subamine-bonded COFs, formed by the acetic

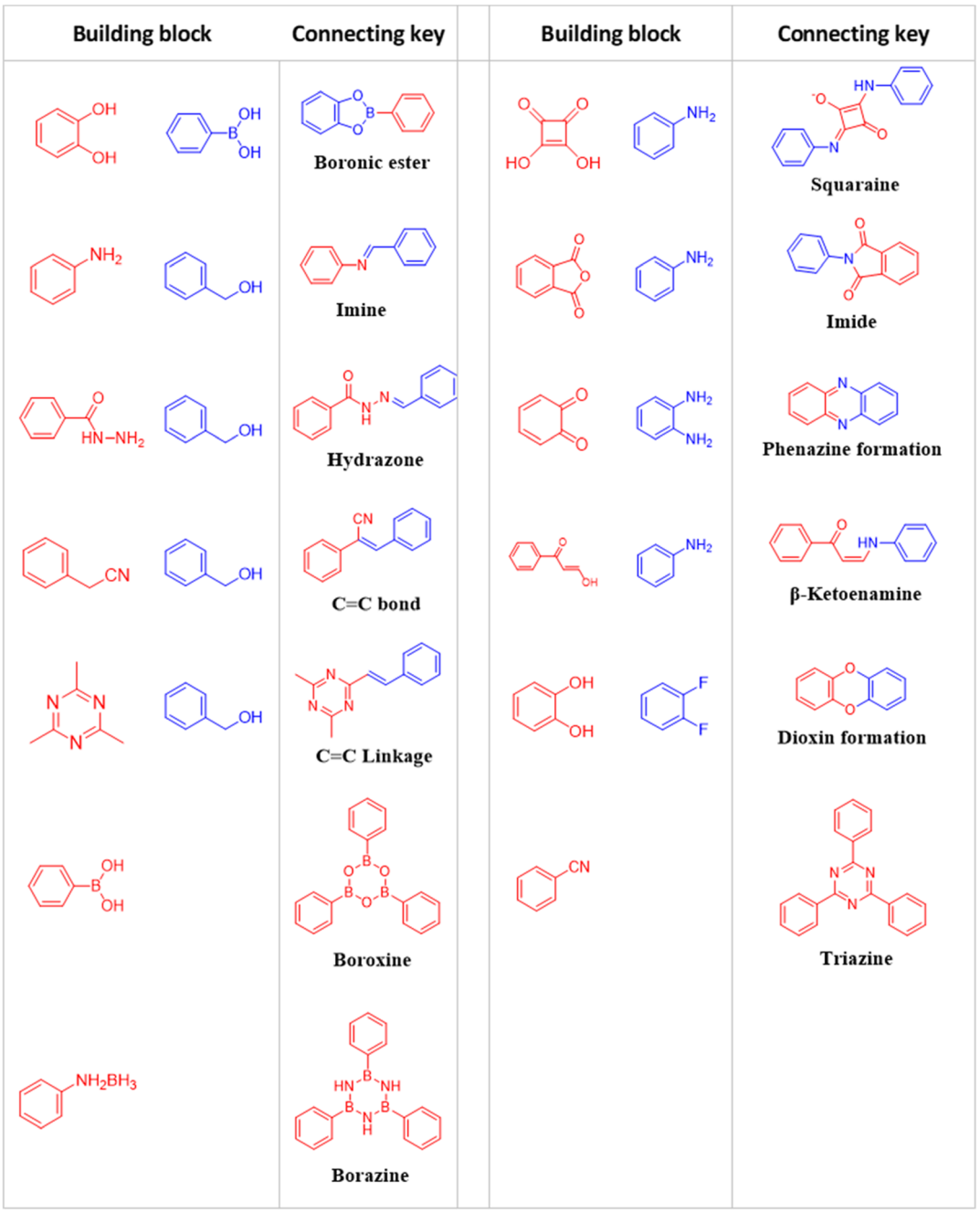

Fig. 1 Typical reversible covalent linkage formation reactions involved in construction of COFs.

acid-catalysed reaction of *o*-tetrahedral structures of tetrakis(4-phenylamino)methane and terephthalaldehyde. X-ray diffraction (XRD) and simulation studies showed that the COFs had a crystalline structure with a five-fold interpenetrating diamond topology. Nitrogen adsorption experiments showed that the material had a Brunauer–Emmett–Teller (BET) specific surface area of 1360 $m^2 g^{-1}$. Since then, many imine-linked COFs have been synthesised, and imine bonding is currently the most widely used COF construction method because of its unique reversibility and tolerance to harsh environments.

Alkene bonding. Alkene-linked COFs have a fully π-conjugated sp^2-carbon backbone, which enables the materials to interact uniquely with photons, electrons, spins, and holes to achieve optoelectronic properties not found with other linkage types. In 2017, Jiang *et al.*[57] used tetrakis(4-formylphenyl)pyrene and *p*-phenylenediacetonitrile as raw materials in sodium hydroxide catalysis to obtain the first example of an alkene-linked COF. In 2019, Yaghi *et al.*[58] reported the construction of a COF without substituent alkene bonding by an alkali-catalysed alcohol–formaldehyde condensation reaction using 2,4,6-trimethyl-1,3,5-triazine and biphenyl dicarboxaldehyde as

the raw materials. The resultant COF maintained good crystallinity under harsh conditions such as strong acids and bases. Another method of constructing COFs without substituent alkene bonding was developed by Feng *et al.*[59] in 2020, which utilised the Horner–Wadsworth–Emmons reaction of phosphoryl diethyl esters with aldehyde groups. Compared with amine-linked COFs, alkene-linked COFs have better thermal stability and photophysical properties. However, their synthesis is more challenging and they tend to have low crystallinity; therefore, there are fewer related studies on alkene-linked COFs than on amine-linked COFs.

The above discussion presented various linkage motifs that have been designed related to the COF production. The COFs linked by covalent bonds show enhanced stability compared to traditional COFs based on boroxine and boronate ester linkages, which makes them have a better prospect in the field of photocatalysis. Therefore, the rational design and development of COF photocatalysts with improved water- and photostability is the key point to realize practical application.

Synthesis of COFs

Most COFs are produced from monomers by reversible condensation reactions of predetermined functional groups. The linkages decompose and readjust during the reaction to produce crystalline COFs. This section introduces various methods for fabricating COFs, such as solvothermal, ionothermal, microwave, mechanochemical, and ultrasonochemical syntheses (Fig. 2).

Solvothermal synthesis

Solvothermal synthesis is one of the most commonly used methods for preparing COFs. This is similar to the synthesis of zeolites and MOFs in an autoclave. In 2005, Yaghi[12] successfully synthesised the first COF by a solvothermal process in a sealed Pyrex tube. Since then, solvothermal methods have been widely used to synthesise COFs. Solvothermal methods enable the mild and controlled synthesis of COFs with good crystallinity and uniform particle size. The COF linkages decompose and condense in the solvent during the heating process. Because the solvent is constantly adjusted, its selection is crucial for effective solvothermal synthesis. Furthermore, the confined reaction environment ensures the involvement of H_2O, which improves the crystalline growth of COFs. The atmosphere is also an influencing factor, similar to the solvent. If the monomer is susceptible to oxidation, an inert gas environment is required to protect it. Although solvothermal syntheses are widely used for producing COFs, they require high temperatures and pressures and long reaction times, which are not conducive to large-scale production. However, large-scale production is possible; for example, Zhao *et al.*[60] explored the continuous flow synthesis of COFs at room temperature to achieve large-scale production.

Another drawback of solvothermal methods is that the synthesised COFs are typically in solid powder form, which limits their applications. However, COF films can also be prepared using the solvothermal method. For example, Dichtel *et al.*[61] used the solvothermal method to synthesise films of COFs and monolayer graphene *via* the condensation of 2,3,6,7,10,11-hexahydroxytriphenylene propylene and 4,40-diphenylbutadiene (boronic acid).

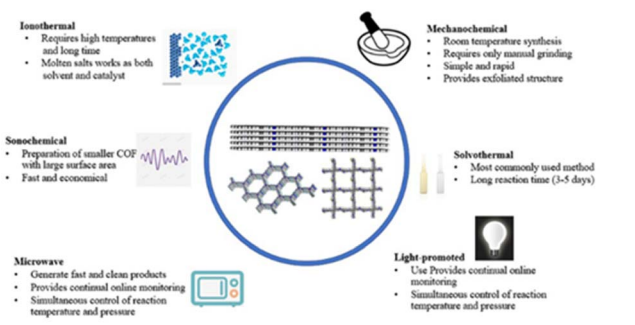

Fig. 2 Common synthesis methods of COFs.

Ionothermal synthesis

The reaction conditions of ionothermal methods are more demanding than those of solvothermal methods. The solvent, such as a salt or ionic liquid, must achieve a certain temperature and pressure. For example, Thomas *et al.*[62] synthesised COFs by the trimerisation of cyano groups in molten $ZnCl_2$, requiring a temperature of 400 °C to reach the molten state. The crystallinity and stability of COFs synthesised by ionothermal methods are more general, and the reaction conditions are more demanding. However, researchers have shown that ionothermal syntheses can take place at room temperature under normal pressure, which take only 12 h; notably, this is a significant reduction in reaction time compared to that for solvothermal methods.[63]

Microwave synthesis

Microwave synthesis methods are a subset of solvothermal synthesis with the application of microwave heating. Compared to traditional solvothermal methods, which use external heating, microwave syntheses use microwave heating to heat the object itself, thereby achieving uniform heating in a short timeframe. Therefore, this method has a short reaction time and good controllability. Microwave heating can improve the reaction rate and accelerate the generation of covalent bonds. For example, Cooper *et al.*[64] synthesised COF-5 by solvothermal and microwave synthesis methods; while the solvothermal synthesis required a reaction time of 72 h, an equivalent product was achieved by microwave synthesis after only 20 min, which corresponds to a more than 200-times shorter reaction time. Furthermore, microwave syntheses do not require the reactants to be in a confined space, and microwave extraction purifies the COFs so that they are almost the same as those obtained using solvothermal methods. Dong *et al.*[65] synthesised stable imine-linked TAPB–TFA-COFs (TAPB = 1,3,5-tris(4-aminophenyl)benzene; TFA = 2,3,5,6-tetrafluorobenzaldehyde) with good crystallinity and a high specific surface area by microwave synthesis with a reaction time of just 2 h.

Mechanochemical synthesis

Mechanochemical synthesis is a widely used synthesis method because it is fast, solventless, and environmentally friendly. In 2013, Banerjee[66] reported the rapid synthesis of COFs by a Schiff reaction *via* milling in a mortar and pestle. The colour of the material gradually changed from orange to red during grinding, and Fourier-transform infrared spectroscopy (FT-IR) confirmed the formation of new covalent bonds. Notably, mechanochemical grinding also exfoliates the COF layers, forming a graphene-like layered structure, unlike solvothermal methods. Recently, Zhou *et al.*[67] successfully synthesised a functionalised COF from an ampholytic polymer, PEIS, by two mechanochemical methods: friction chemistry reaction and ball milling. The prepared functionalised samples were characterised by FT-IR, X-ray photoelectron spectroscopy (XPS), and transmission electron microscopy (TEM), which demonstrated the successful grafting of PEIS onto the COF surface.

Ultrasonochemical synthesis

It is a preferred alternative to conventional solvothermal methods. During ultrasonochemical synthesis, the cavitation effect generates extremely high temperatures and pressures, which are beneficial for the synthesis and crystallisation of COFs. For example, Yang *et al.*[68] synthesised COF-1 and COF-5 using an ultrasonic method with a very short synthesis time. The physical and chemical properties of the prepared materials were comparable to or better than those of materials produced by solvothermal methods. Additionally, ultrasonochemical methods enable the deposition of COFs on materials such as carbon nanotubes (CNTs). Therefore, the ultrasonochemical method is a fast and advantageous synthesis method.

Due to the lack of generally accepted rules for the construction of stable and crystalline COFs, the synthesis of high-quality COFs is still confronted with thorny problems. In addition, the preparation of COFs is confined to the laboratory scale and the searching of appropriate conditions is a tedious job. Therefore, the development of high throughput synthesis methods that are friendly to the environment and simple to operate will be a point of concern.

Application of metal-free COF-based photocatalysts in environmental fields

COFs for photocatalytic hydrogen production

Hydrogen is a clean energy source and an ideal alternative to fossil fuels such as petroleum. The use of solar energy to crack H_2O for hydrogen production is a powerful means of solving the energy crisis and environmental problems caused by the massive consumption of fossil fuels. In recent years, several research studies have analysed COFs used for photocatalytic hydrogen production (Table 1).

In photocatalytic hydrogen production, light irradiation causes the separation of electrons (e^-) and holes (h^+), which then migrate to the surface of the photocatalyst where they partake in reduction and oxidation reactions to generate hydrogen and oxygen:

$$2H^+ + 2e^- \rightarrow H_2 \quad (1)$$

$$H_2O + 2h^+ \rightarrow 2H^+ + 1/2O_2 \quad (2)$$

$$H_2O \rightarrow H_2 + 1/2O_2 \quad (3)$$

Based on the Gibbs free energy change of the overall reaction (eqn (3)), the energy barrier for H_2O cracking is 1.23 eV. Therefore, the material should have a band gap of at least 1.23 eV.

As shown in Fig. 3, Su *et al.*[72] introduced non-metallic S into a COF backbone, along with Pt as a hydrogen precipitation co-

Table 1 The summary of photocatalytic H_2 production performance of COFs

Catalyst	Light irradiation	Co-catalyst	Mass [mg]	Sacrificial donor	HER [μmol h^{-1} g^{-1}]	Ref.
A-TEBPY-COF	AM 1.5G	2.2 wt% Pt	10	10 vol% TEOA	98	69
A-TENPY-COF	AM 1.5G	2.2 wt% Pt	10	10 vol% TEOA	22	69
A-TEPPY-COF	AM 1.5G	2.2 wt% Pt	10	10 vol% TEOA	6	69
OB-POP-1	>420 nm	3 wt% Pt	50	10 vol% TEOA	6.7	70
OB-POP-2	>420 nm	3 wt% Pt	50	10 vol% TEOA	29.9	70
OB-POP-3	>420 nm	3 wt% Pt	50	10 vol% TEOA	45.4	70
OB-POP-4	>420 nm	3 wt% Pt	50	10 vol% TEOA	31.0	70
CN/TMP	Xenon lamp 200–1100 nm	H_2PtCl_6	50	10 vol% TEOA	2057.6	71
$CTFS_{10}$	>420 nm	H_2PtCl_6	20	10 vol% TEOA	2000	72
BP/CTF	>400 nm	3 wt% Pt	50	10 vol% TEOA	42	73
TpBD-COF–CN	>420 nm	3 wt% Pt	30	Sodium ascorbate	384.07	74
TFPT-COF	>420 nm	2.2 wt% Pt	20	Sodium ascorbate	230	75
g-C_3N_4–COF	>420 nm	2 wt% Pt	100	10 vol% TEOA	10 058	76
TpPa-COF–H	>420 nm	H_2PtCl_6	10	Sodium ascorbate	1560	77
TpPa-COF–$(CH_3)_2$	>420 nm	H_2PtCl_6	10	Sodium ascorbate	8330	77
TpPa-COF–NO_2	>420 nm	H_2PtCl_6	10	Sodium ascorbate	220	77
TP–EDDA	>395 nm	H_2PtCl_6	50	10 vol% TEOA	324 ± 10	32
TP–BDDA	>395 nm	H_2PtCl_6	50	10 vol% TEOA	30 ± 5	32
TpDTz COF	>420 nm	10 wt% Ni	5	10 vol% TEOA	941	78

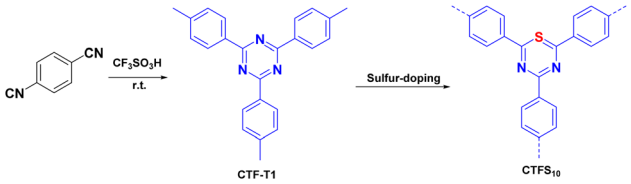

Fig. 3 Synthesis of CTF-T1 and sulfur-doped CTF-T1.

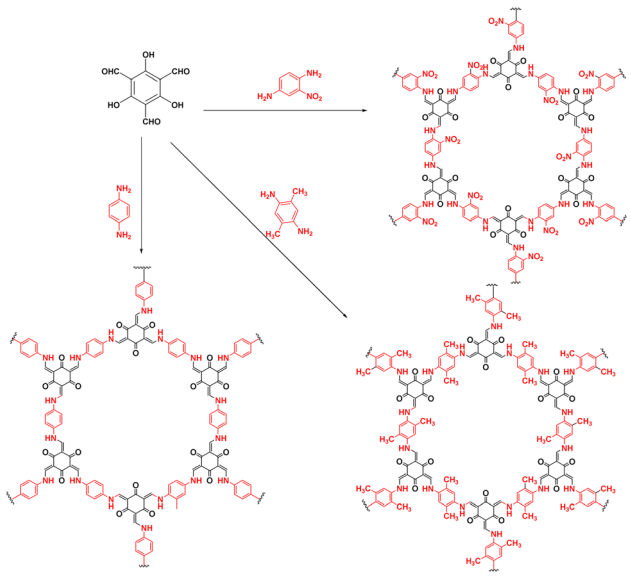

Fig. 4 Synthesis of three COFs with identical principal skeletons (TPA-COF–X, where X = H, $(CH_3)_2$, or NO_2).

catalyst and triethanolamine as an electron donor, which enhanced the photocatalytic hydrogen production rate five-fold compared to that of the original COF. Notably, the hydrogen precipitation rate under light irradiation reached 2000 μmol g^{-1} h^{-1}. This study demonstrated that the introduction of heteroatoms could improve the catalytic performance, enhance the visible light absorption range, reduce electron–hole recombination, and accelerate electron–hole separation. Sun *et al.*[77] synthesised three COFs (TpPa-COF–X, where X = H, $(CH_3)_2$, or NO_2) with the same main framework by choosing trimethyl *m*-phenylene triol and biphenyldiamine as the base monomers (Fig. 4). The relationship between the side-chain functional groups and photocatalytic performance was investigated, which demonstrated that adding suitable functional groups to COFs can enhance their charge separation efficiency and photocatalytic hydrogen production performance. Thomas introduced[32] diacetylene groups into COFs to improve their photocatalytic performance compared to that of monoacetylated COFs (Fig. 5). In addition, COF catalysts without any heteronuclear molecular groups (triazines or heptazines) were successfully used for photocatalytic hydrogen production for the first time.

Lotsch *et al.* were the first to apply COFs to photocatalysis. They proposed three fully planar COFs extended by alkynes, where the corresponding photocurrent effect was enhanced by the alkynes. Additionally, COFs with a lower N content in the donor unit had higher conduction band energy levels, resulting in an increased thermodynamic driving force for H^+ reduction and higher hydrogen precipitation rates.[69]

The introduction of substances such as C_3N_4 into COFs to form heterojunctions has long been a means of enhancing the photocatalytic performance and strengthening electron–hole separation. For example, Li *et al.*[74] investigated the hydrogen production capability of heterojunctions with different ratios of COFs and C_3N_4. The respective advantages of COFs and C_3N_4 were retained while the high porosity and high specific surface area of the COF enhanced the electron–hole separation efficiency. The photocatalytic performance of the heterojunction with the best ratio of COFs and C_3N_4 and a Pt co-catalyst reached 12.8 mmol g^{-1} h^{-1} in the presence of ascorbic acid and a buffer solution. Notably, this value is 62- and 284-times higher than those of the bare COFs and C_3N_4, respectively. Additionally, the apparent quantum efficiency was as high as 15.09%, greatly enhancing the photocatalytic hydrogen production rate. Lin[73] combined black phosphorus (BP) and COFs through a liquid stripping method to enhance the visible light absorption range and charge carrier separation efficiency, which significantly improved the photocatalytic performance of the material. Thus, this study introduced a new approach for the synthesis of metal-free photocatalysts for solar-to-chemical energy conversion.

These studies strongly suggest that taking full advantage of the designability of the COF skeleton structure and coupling COFs with semiconductor photocatalysts to form heterojunction photocatalysts is also a promising strategy. The obtained composites can make full use of the advantages of each component to maximize the photocatalytic performance.

COFs for photocatalytic CO_2 reduction

Fossil fuels are non-renewable energy resources that are widely used in modern society. However, their massive consumption has dramatically increased CO_2 emissions, causing a greenhouse effect and increasing global temperatures. The conversion of CO_2 into energy or other useful substances is crucial to mitigate climate change and reduce the demand for fossil fuels. This strategy can be achieved by converting CO_2 into CO, methane, formic acid, methanol, and other alkanes through photocatalysis using COFs. A comparison of the previously reported metal-free COF photocatalysts applied in CO_2 photoreduction is provided in Table 2.

In 2016, Baeg *et al.*[79] reported a breakthrough in the application of COF-based materials for CO_2 photoreduction. They used the condensation of melamine with perylene diimide to generate a 2D covalent triazine framework (CTF) for CO_2 photoreduction to formic acid under the irradiation of a 450 W xenon lamp. Subsequently, in 2018, Zhu *et al.* proposed the design of two azide-based COFs (ACOF-1 and N_3–COF) without any sacrificial reagents and H_2O as the proton source. These materials reduced CO_2 to methanol with a yield of 13.7 μmol g^{-1}. Although azide COFs do not have high reactivity, pure COF-based materials have been proposed on a theoretical basis for

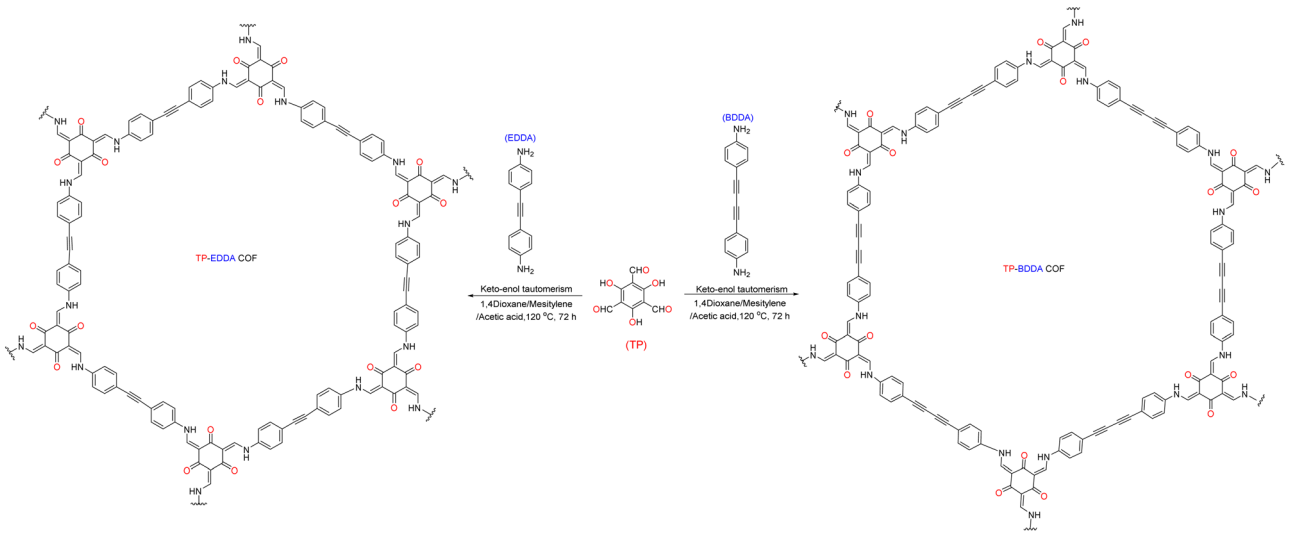

Fig. 5 Synthesis of TP–EDDA and TP–BDDA COFs.

the practical study of CO_2-reducing photocatalysts.[80] In 2019, Wang *et al.*[81] developed a donor–acceptor-type CTF containing trianiline as the electron donor and triazine as the electron acceptor. This optimised the band gap and facilitated visible-light trapping and the migration of photogenerated carriers. The photocatalytic CO_2 reduction activity under visible-light irradiation was significantly improved compared with that of conventional g-C_3N_4 and the covalent triazine backbone. CO_2 reduction in an acetonitrile solution with $Co(bpy)_3^{2+}$ (bpy = 2,2′-bipyridine) as a co-catalyst and triethanolamine as a sacrificial electron donor showed excellent selectivity.

In 2021, Kong *et al.*[82] designed a COF with a donor–acceptor structure using a carbazole triazine monomer (Fig. 6). Density functional theory calculations showed that the triazine structure likely acts as an active site for photocatalysis. The COF was capable of reducing CO_2 at a rate of 102.7 μmol g^{-1} h^{-1} to produce CO with excellent selectivity. This study demonstrated the application of COFs as metal-free photocatalysts for CO_2 reduction and proposed a strategy for preparing efficient photocatalysts by designing donor–acceptor structures. Baek *et al.*[83] proposed the preparation of two different COF structures, TTzTp and BTzTp, from trisbenzothiazole triamine (TTz) or bisbenzothiophene diamine (BTz) monomers with trimethylene resorcinol (Tp). Although BTzTp had a smaller visible-light absorption region and wider band gap, it was more efficient for reducing CO_2 to CO. This was attributed to its greater crystallinity and higher specific surface area, along with a stronger photocurrent and reduced electron–hole recombination. The authors proposed that more factors must be considered in the design and fabrication of COFs as photosensitisers, and new insights were provided for COF design.

Organic semiconductor polymers such as C_3N_4 are promising photocatalysts for the reduction of CO_2. However, there are many limitations. For example, C_3N_4 suffers from extremely severe photogenerated carrier recombination, which significantly affects its photocatalytic activity. Therefore, combining

Table 2 Metal-free COFs applied in the photoreduction of CO_2

COF	Light source	Sacrificial agent	Photosensitizer	Product	Yield (μmol g^{-1} h^{-1})	Ref.
CTF	450 W Xe lamp ($\lambda \geq 420$ nm)	None	$Rh[Cp^*Rh(bpy)H_2O]^{2+}$	HCOOH	881.3×10^3	79
N_3–COF	500 W Xe lamp ($420 \leq \lambda \leq 800$ nm)	None	None	CH_3OH	0.57	80
ACOF-1	500 W Xe lamp ($420 \leq \lambda \leq 800$ nm)	None	None	CH_3OH	0.36	80
DA-CTF	$\lambda \geq 420$ nm	TEOA	$Co(bpy)_3^{2+}$ (bpy = 2,2′-bipyridine)	CO	154.8	81
CT-COF	300 W Xe lamp ($\lambda > 420$ nm)	None	None	CO	102.7	82
TTzTp	Xe lamp ($\lambda = 420$ nm)	TEOA	$Re(CO)_5Cl$	CO	1002	83
BTzTp	Xe lamp ($\lambda = 420$ nm)	TEOA	$Re(CO)_5Cl$	CO	586	83
CTF–BP	$\lambda > 420$ nm	None	None	CH_4	7.81	84
COF-TD	Xe lamp	H_2O	None	CO/CH_4	7.08/2.37	85
TpBD–H_2	800 nm $\geq \lambda \geq$ 420 nm	TEOA	None	HCOOH	45.7	87
TpBD–$(CH_3)_2$	800 nm $\geq \lambda \geq$ 420 nm	TEOA	None	HCOOH	86.3	87
TpBD–$(OCH_3)_2$	800 nm $\geq \lambda \geq$ 420 nm	TEOA	None	HCOOH	108.3	87
TpBD–$(NO_2)_2$	800 nm $\geq \lambda \geq$ 420 nm	TEOA	None	HCOOH	22.2	87
TAPBB	1000 nm $\geq \lambda \geq$ 420 nm	None	None	CO	24.6	89

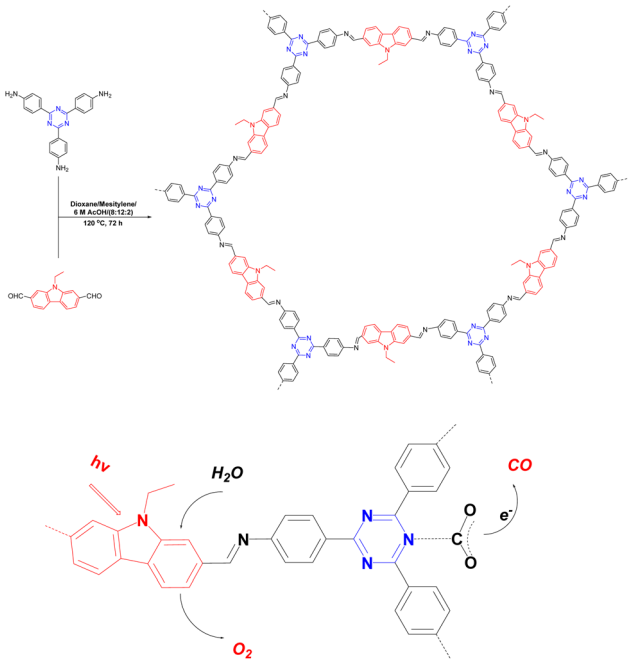

Fig. 6 Schematic diagram of CT-COF synthesis and the mechanism of CO_2 reduction.

COFs with C_3N_4 to generate heterojunctions is an ideal method of enhancing the photocatalytic performance. Zhong *et al.*[84] were the first to propose a combination of BP and CTF to prepare BP–CTF heterojunctions for CO_2 photoreduction, which significantly enhanced the CO_2 reduction rate. Under visible-light irradiation, the rates of CO and CH_4 production were 4.60 and 7.81 μmol g^{-1} h^{-1}, respectively. This study demonstrated the potential of metal-free selective photocatalysts with heterogeneous structures. In 2020, Yang *et al.*[85] proposed a method of enhancing the CO_2 photoreduction performance by combining CN with a COF to prepare 2D CN–COF without sacrificial reagents. Under irradiation of a 300 W xenon lamp, the rates of CO and CH_4 production were 7.08 and 2.37 μmol g^{-1} h^{-1}, respectively, which were 9.2- and 3.3-times higher than those of 2D CN and COF-TD.

The introduction of functional groups into COFs leads to structural changes that can reduce the band gap, enhance the charge separation efficiency, increase the visible-light absorption range, and improve the photocatalytic activity. Therefore, this method is promising for achieving better CO_2 photoreduction. It is also used for the reduction of CO_2 and NADH. Among the functionalised COFs, COF-4 is highly reactive and capable of reducing CO_2 to formic acid at a rate of 150.8 μmol g^{-1} h^{-1} (Fig. 7).[86] Fan *et al.*[87] used TP and BD to explore the

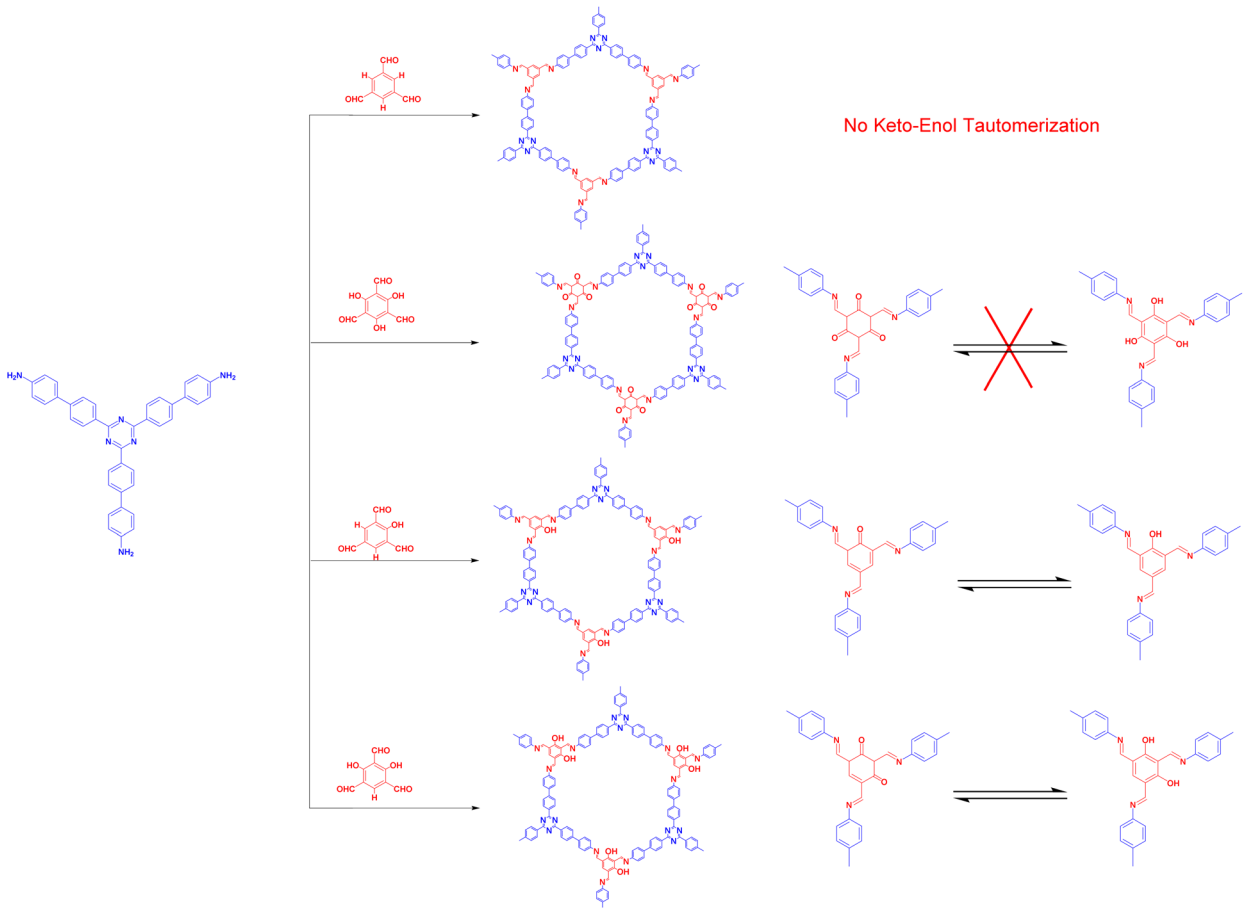

Fig. 7 Systematic Synthesis and Structures of COFs 1–4.

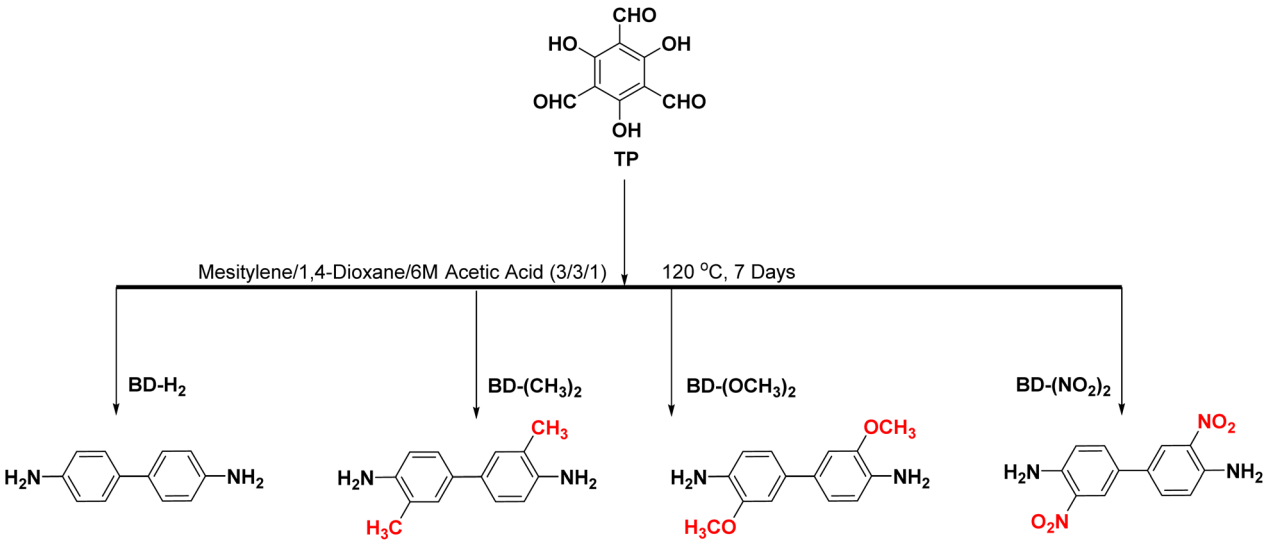

Fig. 8 Schematic diagram of the synthetic path for TpBD–X [X = $-H_2$, $-(CH_3)_2$, $-(OCH_3)_2$, and $-(NO_2)_2$].

effect of different functional groups toward photocatalytic CO_2 reduction (Fig. 8). The functional groups were introduced on the side chains of the COFs, which resulted in differences in the morphology, absorption wavelength, and band gap. It was proposed that functionalisation with electron-donating groups can strengthen the conjugation effect within COFs and accelerate photogenerated charge separation and transfer, thereby enhancing the CO_2 photoreduction performance.

The halogenation of organic semiconductors is a common method of modulating the energy band structure. Among the halogens, Br is of particular interest because of its excellent photoreceptivity.[88] Su *et al.*[89] found that the difference between the conduction band of COF-366 and the CO/CO_2 redox potential was 0.35 V; therefore, the reduction reaction occurred easily. However, the difference between the valence band and O_2/H_2O redox potential was very small (0.04 V), which meant that the oxidation reaction was difficult to achieve. A bottom-up strategy was proposed to adjust the band gap of the COF by introducing Br to raise the valence band and make it favourable for the oxidation reaction (Fig. 9). The yield of TAPBB-COF for CO_2 reduction to CO under simulated sunlight irradiation with only H_2O as the electron donor was 24.6 μmol g^{-1} h^{-1}, which was roughly three times that of COF-366. In addition, TAPBB-COF exhibited good selectivity and stability. Density functional theory calculations showed that the N atoms in the porphyrin ring and imine bonds and Br atoms played crucial roles in CO_2 reduction.

Although the photoreduction of CO_2 by COFs has been widely investigated, the quantum efficiency of photocatalysis is relatively low compared with other systems, and it is difficult to obtain more valuable hydrocarbon products such as ethane and ethylene. It is expected that more research will focus on the development of more efficient and promising COF-based photocatalysts for CO_2 utilization.

COFs for photocatalytic pollutant degradation

Over the past few decades, environmental problems have become increasingly severe. The pollution from industrial wastewater is a major concern. In this regard, photocatalysis is a powerful tool for the degradation of organic pollutants. The photodegradation mechanism involves the photogenerated production of hydroxyl and superoxide radicals, which are active substances that can degrade organic substances. Many COFs have been used as photocatalytic materials for the efficient and selective degradation of pollutants.

Cai *et al.*[51] synthesised an all-sp^2 carbon 2D-COF by the homogeneous introduction of triazine units through an acid-catalysed aldol reaction. It was applied for the photodegradation of methyl orange (MO) and methylene blue (MB) under visible-light irradiation ($\lambda \geq 420$ nm), and achieved 99% pollutant degradation within 20 min. This excellent performance was attributed to the enhanced electron separation efficiency through carbon–carbon double bond linkages, which promoted the transfer of photogenerated carriers. Subsequently, as shown in Fig. 10, a series of imine-based COFs were prepared (COFA + B, COFA + C, and COFA + D) and used for MO photodegradation in H_2O,[90] and the structure–performance relationship was systematically investigated. After visible-light irradiation for 30 min, COFA + C achieved complete MO degradation, whereas COFA + B degraded only 29.6% of MO and COFA + D degraded almost none, which was primarily due to the higher conjugation and density of the visible-light active centre (triazine ring) in the COFA + C structure. Liu *et al.*[91] prepared an amide-bonded COF with an electro-spun membrane that exhibited excellent photoelectric properties. Notably, the metal-free membrane performed better than a C_3N_4 photocatalyst mixed with metal, with superior photodegradation activity for rhodamine B (RhB) in H_2O under sunlight irradiation.

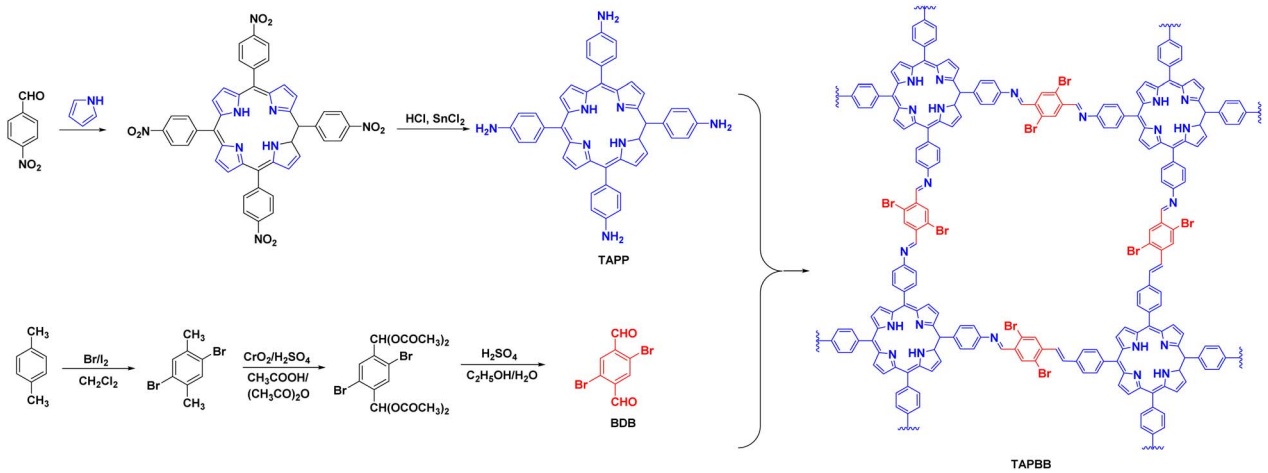

Fig. 9 Synthesis route of TAPBB-COF.

Qiu *et al.*[92] constructed various vinyl-linked COFs from diacetylene and triazine units for the photocatalytic degradation of organic pollutants (Fig. 11). The vinyl-linked COFs exhibited excellent photocatalytic activity and ultra-high stability. Additionally, the recombination of photogenerated carriers was inhibited by the acetylene group. The prepared COFs were able to degrade more than 96% of phenol and norfloxacin pollutants within 15 min. Furthermore, the COFs were reused for at least five degradation cycles with almost no loss of degradation performance. Alemán *et al.*[93] designed a series of

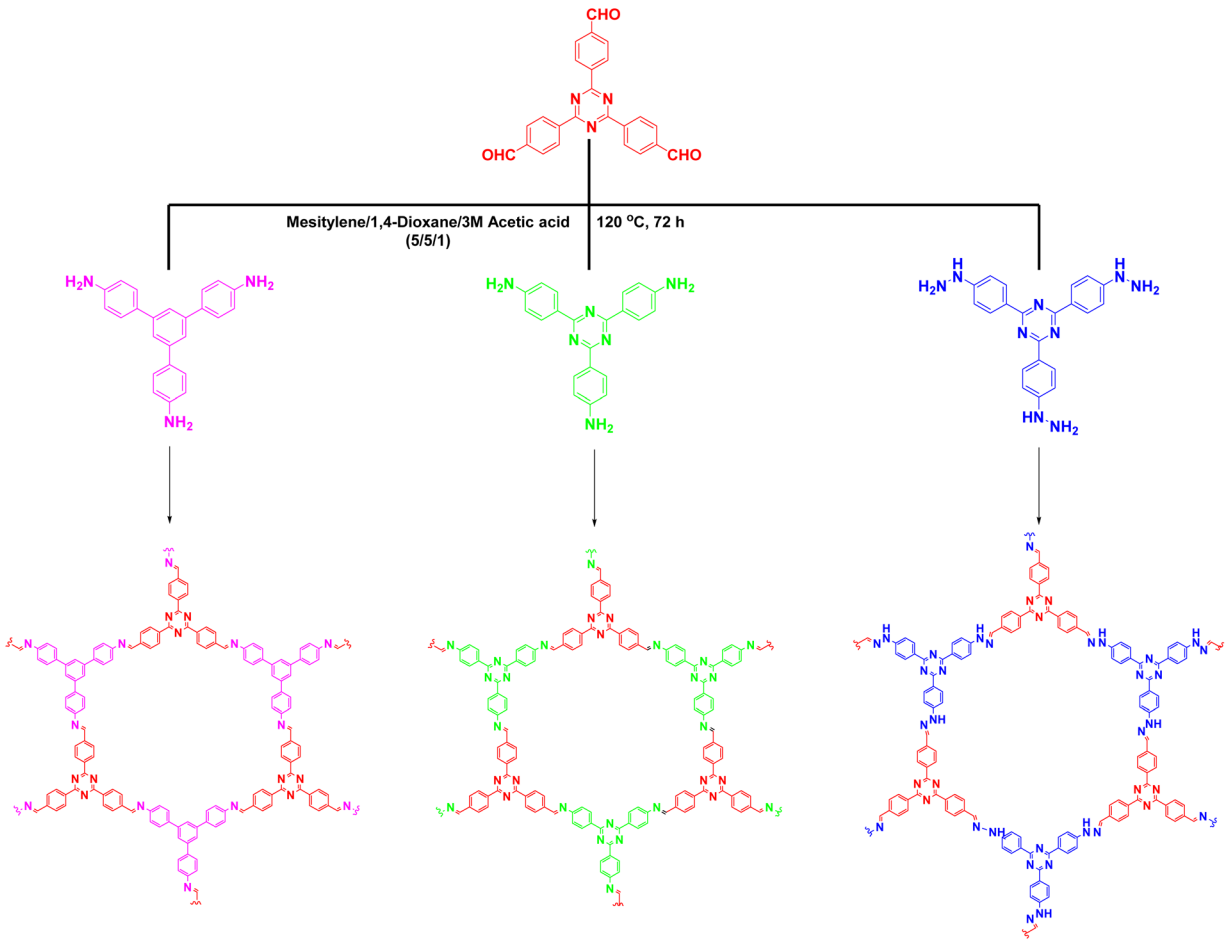

Fig. 10 COFs were synthesized by reaction of different nitrogenous building blocks with 4,4′,4″-(1,3,5-triazine-2,4,6-triyl) Schiff bases.

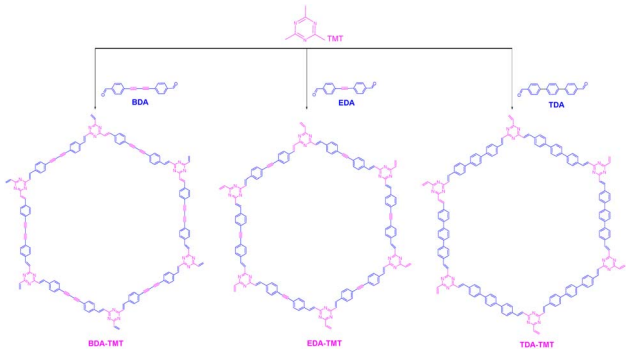

Fig. 11 Strategy for preparing BDA–TMT, EDA–TMT, and TDA–TMT.

COFs from different combinations of monomer pairs as photocatalysts for the degradation of specific pollutants by different pathways (Fig. 12). Different monomer ratios were used to degrade different pollutants, and three pollutants (PBDE-1, Sudan Red III, and MB) with different properties were effectively photodegraded. The authors reported that the energy transfer efficiency of processes initiated by different substances was dependent on the monomer ratios. This study extended the application of COFs for selective pollutant degradation to a wide range of photocatalytic transformations. Chen *et al.*[94] reported triazine-based sp^2-carbon conjugated g-C_{18N_3}-COFs for the efficient photocatalytic degradation of RhB and detection of pH. The prepared COFs had good photocatalytic performance owing to their protonated broadened light absorption region and narrow band gap.

Combining COFs with other photocatalytic materials can enhance the photochemical performance. For example, in 2017, Cai[50] proposed the integration of g-C_3N_4 into COFs, which introduced multiple functional groups and an ordered donor–acceptor structure, thereby enhancing the photocatalytic performance, photoinduced electron transfer, and charge separation efficiency. The chemical activity of the C_3N_4-embedded COFs was greatly enhanced compared to that of conventional C_3N_4 and COFs. After 40 min of light exposure, MO was almost completely decomposed by the COFs, whereas there was almost no change in the MO concentration when using pure g-C_3N_4. Furthermore, Tan *et al.*[95] reported the construction of new porous carbides (PCN-1 and PCN-2) by embedding heptazine building blocks into COFs (Fig. 13). Unlike the previous study by Cai,[50] Tan *et al.* combined g-C_3N_4 with triazine COFs to form PCN-2, rather than embedding C_3N_4 alone. A comparison of PCN-1, PCN-2, and triazine-based COFs for the degradation of RhB showed that the reactivity of PCN-2 was 15 times higher than that of PCN-1 and 1.8-times higher than that of the triazine COFs.

In 2021, Wang *et al.*[96] prepared COF/CNT composite membranes, in which the CNTs provided a large specific surface area and photothermal effect, and the COFs enhanced the mechanical properties and hydrophilicity of the CNTs. Thus, the composite membranes had improved photocatalytic activity owing to the positive interaction between the COFs and CNTs. The composite membranes showed excellent degradation ability for Mordant Black 17 (MB17) and strong practicality. The total degradation ability of the COF/CNT membranes reached 708.2 mg g^{-1}, and they could be reused seven times with only 10.6% loss of performance. Notably, the use of composite membranes eliminates the problems associated with recovering traditional powder photocatalysts from water bodies, increasing their real-world applicability. Tong *et al.*[97] reported the synthesis of COFs with g-C_3N_4 active centres by ball milling. The prepared photocatalyst was employed for the photodegradation of sulfathiazole with good reusability. In industrial wastewater, it was able to effectively degrade organic pollutants even in the presence of interference from other substances in solution. These studies by Wang *et al.*[98] and Tong *et al.*[99] reveal the enhanced degradation of pollutants through the synergistic effects of COFs and peroxymonosulfate (PMS6).

Interestingly, Giesy[100,101] proposed the preparation of COFs for the degradation of pollutants in large quantities by using ball milling, which could possibly be applied in industrial production.

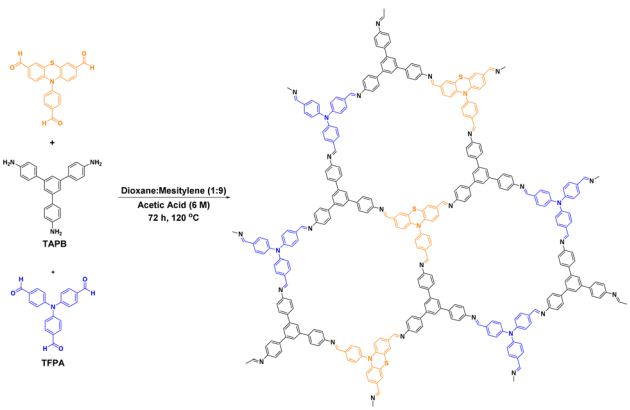

Fig. 12 Synthesis of a series of materials with different TFPA/3 molar ratios.

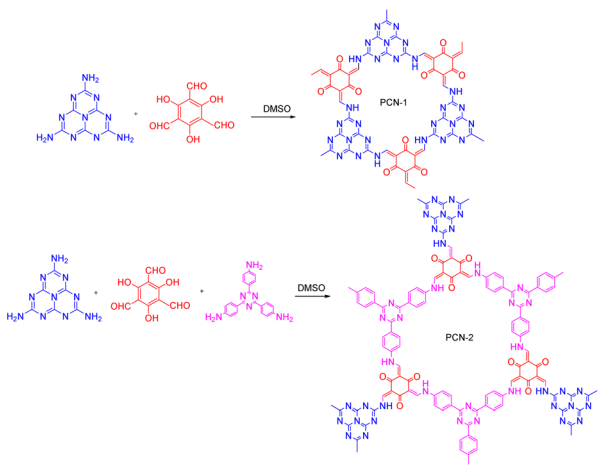

Fig. 13 Synthesis route of PCN-1 and PCN-2.

COFs for photocatalytic organic synthesis

The use of COFs as photocatalysts to drive chemical reactions under visible light irradiation has emerged as a viable option for the synthesis of organic compounds. This method is advantageous because it requires only mild conditions and has high selectivity and reusability. Despite the negative reputation of CO_2 in light of climate change, it remains an extremely valuable resource for its conversion into beneficial substances. To achieve this, its chemical fixation is crucial.

In 2016, Bhanage[102] proposed the synthesis of two novel COFs, 2,3-DhaTph and 2,3-DmaTph, for the reaction of CO_2 with epoxide rings. These COFs contain hydrogen bond donating groups, which accelerate the addition reaction of CO_2 with epoxide rings, as well as phenolic hydroxyl groups, which create intramolecular hydrogen bonds with the nearby imine bonds. Therefore, these COFs effectively catalyse the reaction of CO_2 with epoxide rings. Additionally, porphyrin groups with abundant N-active sites greatly enhance the photocatalytic performance. The general effect of using only catechol as the catalyst indicates that the high specific surface area of the material also plays a crucial role, in that it provides more reaction sites. Consequently, 2,3-DhaTph and 2,3-DmaTph afford high yields and selectivity. Furthermore, a new method for the immobilisation of CO_2 under metal- and solvent-free conditions was provided. Later, in 2018, Liu *et al.*[103] adopted a bottom-up strategy by introducing hydroxyl groups into COFs. The prepared COFs had many N-active sites in the abundant pore channels, and hydroxyl groups that activated epoxy compounds by forming intermolecular hydrogen bonds. The N-rich structures also facilitated the adsorption of CO_2. With the use of the co-catalyst TBAB, the metal-free organic catalyst exhibited good substrate adaptability under mild conditions and catalytic performance for cycloaddition reactions of CO_2 with epoxides.

Islam *et al.*[104] reported the construction of a highly crystalline and stable 2D-COF with a very low band gap for the carboxylation of unsaturated olefins with CO_2. The COFs were synthesised by Schiff base condensation using trimethyl resorcinol

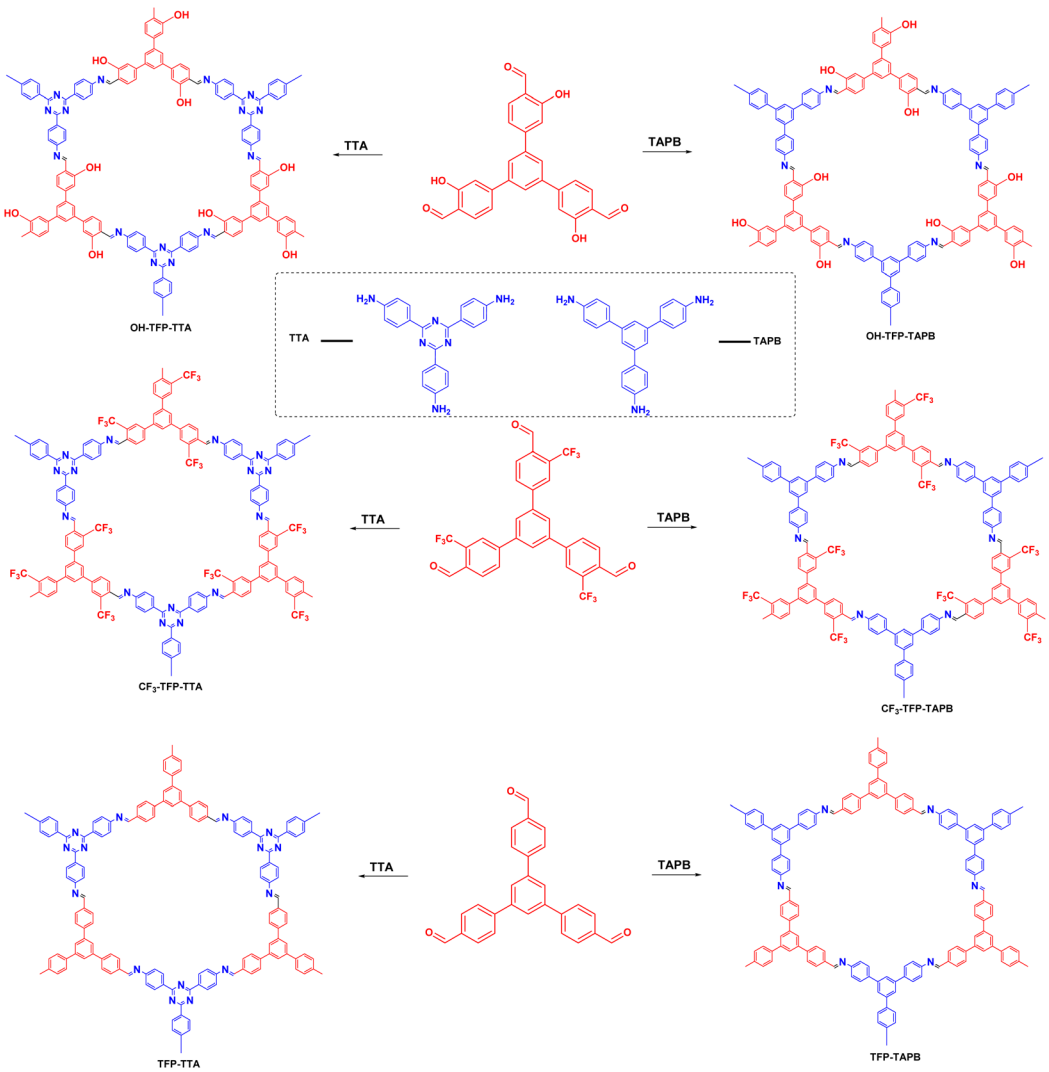

Fig. 14 Illustration of the synthesis of [3 + 3] COFs with different compositions.

and *o*-toluidine as building blocks. The carboxylation of styrene and other analogues was carried out using the electron donor triethylamine and co-catalyst *p*-terphenyl under light-emitting diode (LED) illumination. The performance of the photocatalyst did not significantly decrease even after several reaction cycles, providing a new method for carbon sequestration in organic reactions and greatly improving the efficiency of CO_2 utilisation.

Organobromide compounds are often produced during the production of organic chemicals with Br catalysts. Many organobromides have an adverse environmental effect and are considered persistent organic pollutants (POPs), similar to organochlorides. In 2020, Yang *et al.*[105] proposed a series of 2D-COFs based on different substituents of 1,3,5-tris(4-formylphenyl)benzene, 4,4′,4-(1,3,5-triazine-2,4,6-triyl) triphenylamine and 1,3,5-tris(4-aminophenyl)benzene. The effects of the different substituents on the material properties were investigated (Fig. 14). Among the prepared COFs, OH–TFP–TTA had a very high specific surface area, very low band gap, excellent electron separation efficiency, and high photoresponsive current. Moreover, in photoinduced dehalogenation reactions, it exhibited very high photocatalytic performance with a reaction yield of 90%. The hydroxyl group activated the nearby amino group, which greatly enhanced the photocatalytic performance of the COF.

COFs have been used in photoinduced radical polymerisation reactions. Thomas *et al.*[106] were the first to report two donor–acceptor-structured COFs for the visible light catalysis of methyl methacrylate to polymethyl methacrylate. Notably, the non-homogeneous COF catalysts were easily separated after the reaction and could be reused multiple times. Subsequently, Hou *et al.*[107] and Li *et al.*[108] reported the use of COFs in photoinduced radical polymerisation reactions and obtained excellent results.

As the study of COFs for photocatalytic organic synthesis is still in its infancy, the mechanism of photocatalytic reaction is not clear enough and needs further exploration. It remains a big challenge to design COF photocatalysts according to the demand of organic reactions.

COFs for photocatalytic environmental remediation

COFs have also been used in environmental remediation. Under light irradiation, electrons and holes migrate to the material surface where they generate highly reactive radical substances that participate in the reduction of heavy metal ions and conversion of toxic and hazardous substances. For example, in 2019, Tan *et al.*[109] reported the synthesis of highly crystalline CTFs by adjusting the monomer feed rate to control crystal growth and improve the crystallinity (Fig. 15). The highly crystalline CTFs had excellent charge transfer efficiency and photogenerated electron–hole pair separation, which was beneficial for photocatalytic applications. The crystalline CTFs had significantly better NO_x removal performance than amorphous CTFs and C_3N_4, with significantly lower by-product production. Thus, the high crystallinity resulted in better photocatalytic performance.

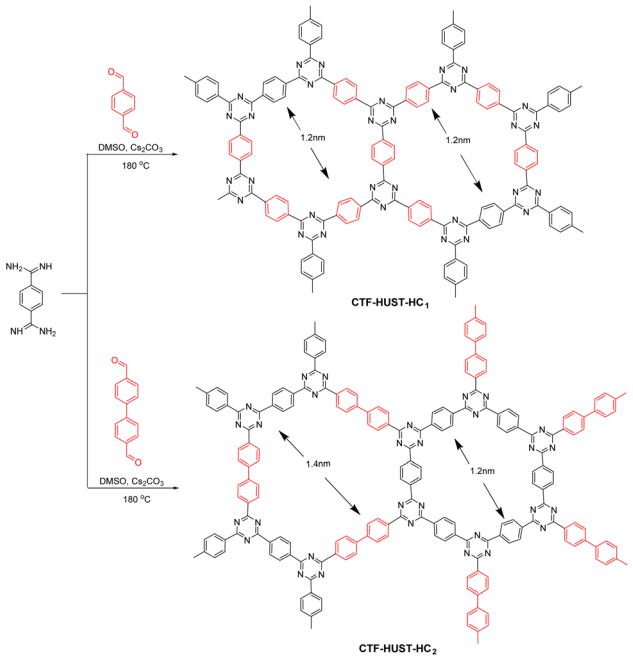

Fig. 15 Synthesis of CTF-HUST-HC_1 and CTF-HUST-HC_2.

In a recent report, Hu *et al.*[110] synthesised COF-TpBpy using tricarbonylresorcinol and bipyridine. Here, bipyridine is a ligand that can coordinate with heavy metal ions to form bipyridine salts, and tricarbonylresorcinol introduces hydroxyl groups into the material. Therefore, TpBpy integrates OH^- and N into the pore wall to capture U(VI) ions. The photoreduction of U(VI) (30 mg L^{-1}) was probed using the photocatalyst TpBpy in air with a xenon lamp with a 420 nm cut-off filter as the light source. The U(VI) removal rate was approximately 76% after 420 min of light exposure. Moreover, this effect did not decrease significantly even after several cycles of testing, indicating that the prepared COFs have high stability and reusability.

Another critical toxin is mustard gas, which has been used as a chemical weapon since World War One (WWI). Therefore, it is important to develop efficient decontamination methods for the removal of mustard gas from the environment. Zang *et al.*[111] reported an amine-linked porphyrin COF with 5,10,15,20-

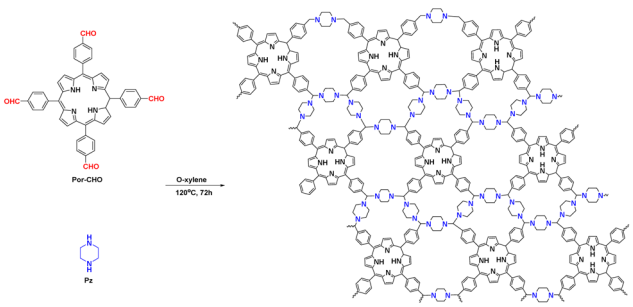

Fig. 16 Synthesis of Por-aminal-COF *via* the condensation of Por-CHO and Pz.

tetrakis(4-benzaldehyde)porphyrin and piperazine as monomers (Fig. 16). The morphology of the COF was examined by scanning electron microscopy and TEM. The COF exhibited an intersystem crossing process with a 2D lamellar stacking morphology, where most of the excited electrons were transferred to the T1 state with a long lifetime. This property greatly enhanced the O_2 generation rate of the prepared photocatalyst and facilitated the removal of 2-chloroethyl ethyl sulfide (CEES). In an O_2 atmosphere with methanol as the solvent, the COF was able to effectively remove CEES under LED visible-light irradiation within 10 min with a $t_{1/2}$ of 5 min. The oxidation of CEES to the less toxic 2-chloroethyl ethyl sulfoxide occurred with 100% selectivity. Moreover, no toxic sulfone derivatives (2-chloroethyl ethyl sulfone) were detected, demonstrating the highly selective partial oxidation ability of this COF.

In 2019, Chen *et al.*[112] reported two COFs with enhanced photocatalytic performance by introducing heteroatoms, such as N or S, and using benzothiadiazole as a monomer (Fig. 17). The COFs were utilised in the reduction of Cr(VI) ions. Among them, TPB–BT-COF was able to reduce more than 99% of Cr(VI) within 75 min, which was attributed to its small band gap and good visible-light absorption efficiency. Later, Ma *et al.*[113] synthesised various N-containing COFs by changing the number and position of heterocyclic N atoms and found that introducing heterocycles in the monomer could optimise the local electronic structure of the COFs and enhance the charge effect. Among them, COF-PMD (containing two heterocyclic N atoms) reduced more than 99% of Cr(VI) in 120 min, whereas COF-PMD (aldehyde in [2,2′-bipyridine]-5,5′-dicarboxaldehyde and 2,4,6-trihydroxybenzene-1,3,5-tricarbaldehyde) removed more than 95% in 20 min.

Zhai *et al.*[114] reported the *in situ* growth of COF–CNNS hybrid materials based on porous C_3N_4 nanosheets (CNNS). Comparing metal hybrids of COFs to the prepared COF–CNNS revealed that they conform to the CHON principle. The reduction of Cr(VI) was carried out under visible-light irradiation, and the COF/CNNS catalyst with the optimal mixing ratio of 20% could remove more than 99% of Cr(VI) in 30 min without the use of a sacrificial agent. In addition, the reduction kinetic constant was 0.141, which is much higher than that of other reported CNNS-based photocatalysts.

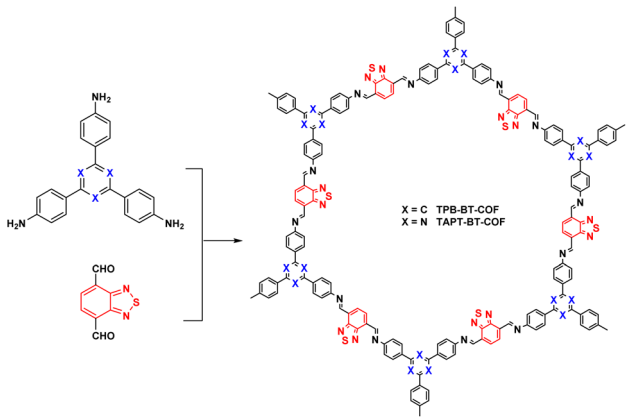

Fig. 17 Synthesis of TPB–BT-COF and TAPT–BT-COF.

The above research studies have demonstrated that COFs are excellent materials for environmental remediation, however, the cost of COF production is still not compromised compared to the existing materials. It is necessary to develop economic and scalable synthetic methods to reduce the cost, promoting the development of COFs for use as the future environmental treatment materials.

Summary and outlook

COFs are an emerging class of multivacancy organic polymers with a large specific surface area, stable pore size, high crystallinity, and good stability. Moreover, the tailorability of the structure provides a theoretical basis for the preparation of various COF-based materials. This paper summarises the applications of metal-free COFs as photocatalysts in environmental fields, including hydrogen and oxygen production, CO_2 reduction, pollutant degradation, environmental remediation, and organic synthesis. Methods for enhancing the photocatalytic performance of COF-based materials are described in detail. Although significant progress and achievement have been made in the field of photocatalysis in recent years, the research on COFs for photocatalytic applications is still in its infancy and several issues should be resolved for future practical applications.

The synthesis of high crystallinity COFs is complicated and time-consuming, which restricts the exploration of photocatalysis and the process of industrial application. A new synthetic method for mass and rapid production of COFs is urgently required. Besides, the recycling stability of COFs is strictly limited by their poor moisture tolerance, therefore the development of moisture-tolerant linkers and reactions to obtain stable COFs is promising. In addition, the photocatalytic efficiency, which is the most important issue concerning photocatalytic hydrogen evolution, oxygen production, and CO_2 reduction is still relatively poor. Thus, the predesign or construction of COFs with expanded light absorption range and rapid charge separation is highly expected. Furthermore, many photoreaction mechanisms still require explanation, so it is challenging to develop well-defined COF-based photocatalysts to uncover the structure–property–activity relationship.

Conflicts of interest

There are no conflicts to declare.

Acknowledgements

This work was supported by the Natural Science Foundation of China (No. 52270039, 51878326, and 22109064) and Natural Science Foundation of Jiangxi Province (No. 20212ACB203007).

References

1 Z. Long, Q. Li, T. Wei, G. Zhang and Z. Ren, *J. Hazard. Mater.*, 2020, **395**, 122599.

2 Z. Ajmal, M. u. Haq, Y. Naciri, R. Djellabi, N. Hassan, S. Zaman, A. Murtaza, A. Kumar, A. G. Al-Sehemi, H. Algarni, O. A. Al-Hartomy, R. Dong, A. Hayat and A. Qadeer, *Chemosphere*, 2022, **308**, 136358.
3 M. Han, S. Zhu, S. Lu, Y. Song, T. Feng, S. Tao, J. Liu and B. Yang, *Nano Today*, 2018, **19**, 201–218.
4 X. Lü, F. Huang, X. Mou, Y. Wang and F. Xu, *Adv. Mater.*, 2010, **22**, 3719–3722.
5 D. Zhang, W. Zheng, R. Lin, Y. Li and F. Huang, *Adv. Funct. Mater.*, 2019, **29**, 1900935.
6 C. H. Mak, X. Han, M. Du, J.-J. Kai, K. F. Tsang, G. Jia, K.-C. Cheng, H.-H. Shen and H.-Y. Hsu, *J. Mater. Chem. A*, 2021, **9**, 4454–4504.
7 H. Zheng, F. Gao and V. Valtchev, *J. Mater. Chem. A*, 2016, **4**, 16756–16770.
8 Y. Chai, W. Dai, G. Wu, N. Guan and L. Li, *Acc. Chem. Res.*, 2021, **54**, 2894–2904.
9 Z. Xu, C. Zhang, L. Huang, Y. Yu, A. Long, Y. An and Y. Gu, *Microporous Mesoporous Mater.*, 2022, **343**, 112143.
10 J. Fonseca, T. Gong, L. Jiao and H.-L. Jiang, *J. Mater. Chem. A*, 2021, **9**, 10562–10611.
11 W. Tu, Y. Xu, S. Yin and R. Xu, *Adv. Mater.*, 2018, **30**, 1707582.
12 A. P. Côté, A. I. Benin, N. W. Ockwig, M. O'Keeffe, A. J. Matzger and O. M. Yaghi, *Science*, 2005, **310**, 1166–1170.
13 H. Fan, A. Mundstock, A. Feldhoff, A. Knebel, J. Gu, H. Meng and J. Caro, *J. Am. Chem. Soc.*, 2018, **140**, 10094–10098.
14 C. Kang, Z. Zhang, A. K. Usadi, D. C. Calabro, L. S. Baugh, K. Chai, Y. Wang and D. Zhao, *J. Am. Chem. Soc.*, 2022, **144**, 20363–20371.
15 P. She, Y. Qin, X. Wang and Q. Zhang, *Adv. Mater.*, 2021, **31**, 2101175.
16 X. Wu, X. Han, Q. Xu, Y. Liu, C. Yuan, S. Yang, Y. Liu, J. Jiang and Y. Cui, *J. Am. Chem. Soc.*, 2019, **141**, 7081–7708.
17 F. Yu, W. Liu, B. Li, D. Tian, J. Zuo and Q. Zhang, *Angew. Chem., Int. Ed.*, 2019, **58**, 16101–16104.
18 F. Yu, W. Liu, S. W. Ke, M. Kurmoo, J. Zuo and Q. Zhang, *Nat. Commun.*, 2020, **11**, 5534.
19 Y. Zhi, Z. Wang, H. Zhang and Q. Zhang, *Small*, 2020, **16**, 2001070.
20 J. Guo and D. Jiang, *ACS Cent. Sci.*, 2020, **6**, 869–879.
21 T. Qiu, Z. Liang, W. Guo, S. Gao, C. Qu, H. Tabassum, H. Zhang, B. Zhu, R. Zou and Y. Shao-Horn, *Nano Energy*, 2019, **58**, 1–10.
22 B. Zhu, R. Zou and Q. Xu, *Adv. Energy Mater.*, 2018, **8**, 1801193.
23 H. Zhang, W. Xia, H. Shen, W. Guo, Z. Liang, K. Zhang, Y. Wu, B. Zhu and R. Zou, *Angew. Chem., Int. Ed.*, 2020, **59**, 1871–1877.
24 Y. Yang, Y. Wang, G. Gao, M. Liu, C. Miao, L. Li, W. Cheng, Z. Zhao, Y. Chen, Z. Xin, S. Li, D. Li and Y. Lan, *Chin. Chem. Lett.*, 2022, **33**, 1439–1444.
25 H. Liu, J. Chu, Z. Yin, X. Cai, L. Zhuang and H. Deng, *Chem*, 2018, **4**, 1696–1709.
26 H. Ding, Y. Wang, M. Liu, J. Shi, T. Yu, Y. Xia, M. Lu, Y. Yang, Y. Chen, S. Li and Y. Lan, *Chem. Mater.*, 2022, **34**, 10752–10760.
27 N. An, Z. Guo, J. Xin, Y. He, K. Xie, D. Sun, X. Dong and Z. Hu, *J. Mater. Chem. A*, 2021, **9**, 16824–16833.
28 T. Wu, Z. Ma, Y. He, X. Wu, B. Tang, Z. Yu, G. Wu, S. Chen and N. Bao, *Angew. Chem., Int. Ed.*, 2021, **60**, 10366–10374.
29 J. Tang, C. Su and Z. Shao, *Small Methods*, 2021, **5**, 2100945.
30 D. Wang, T. Qiu, W. Guo, Z. Liang, H. Tabassum, D. Xia and R. Zou, *Energy Environ. Sci.*, 2021, **14**, 688–728.
31 S. Wan, J. Guo, J. Kim, H. Ihee and D. Jiang, *Angew. Chem., Int. Ed.*, 2008, **47**, 8826–8830.
32 P. Pachfule, A. Acharjya, J. Roeser, T. Langenhahn, M. Schwarze, R. Schomacker, A. Thomas and J. Schmidt, *J. Am. Chem. Soc.*, 2018, **140**, 1423–1427.
33 M. Xu, M. Lu, G. Qin, X. Wu, T. Yu, L. Zhang, K. Li, X. Cheng and Y. Lan, *Angew. Chem., Int. Ed.*, 2022, **61**, e202210700.
34 M. Lu, J. Liu, Q. Li, M. Zhang, M. Liu, J. Wang, D. Yuan and Y. Lan, *Angew. Chem., Int. Ed.*, 2019, **58**, 12392–12397.
35 M. Lu, M. Zhang, J. Liu, T. Yu, J. Chang, L. Shang, S. Li and Y. Lan, *J. Am. Chem. Soc.*, 2022, **144**, 1861–1871.
36 Y. Cheng, W. Ji, X. Wu, X. Ding, X. Liu and B. Han, *Appl. Catal., B*, 2022, **306**, 121110.
37 Y. Zhi, Z. Li, X. Feng, H. Xia, Y. Zhang, Z. Shi, Y. Mu and X. Liu, *J. Mater. Chem. A*, 2017, **5**, 22933–22938.
38 S. Karak, K. Dey, A. Torris, A. Halder, S. Bera, F. Kanheerampockil and R. Banerjee, *J. Am. Chem. Soc.*, 2019, **141**, 7572–7581.
39 J. Yue, Y. Wang, X. Ding, Y. Fan, L. Song, P. Yang, Y. Ma and B. Tang, *Mater. Chem. Front.*, 2022, **6**, 3748–3754.
40 B. Zhang, F. Liu, C. Nie, Y. Hou and M. Tong, *J. Hazard. Mater.*, 2022, **435**, 128966.
41 S. Ghosh, A. Nakada, M. A. Springer, T. Kawaguchi, K. Suzuki, H. Kaji, I. Baburin, A. Kuc, T. Heine, H. Suzuki, R. Abe and S. Seki, *J. Am. Chem. Soc.*, 2020, **142**, 9752–9762.
42 Z. Zhou, C. Bie, P. Li, B. Tan and Y. Shen, *Chin. J. Catal.*, 2022, **43**, 2699–2707.
43 H. Wang, H. Wang, Z. Wang, L. Tang, G. Zeng, P. Xu, M. Chen, T. Xiong, C. Zhou, X. Li, D. Huang, Y. Zhu, Z. Wang and J. Tang, *Chem. Soc. Rev.*, 2020, **49**, 4135–4165.
44 S. Wang, B. Y. Guan, X. Wang and X. W. D. Lou, *J. Am. Chem. Soc.*, 2018, **140**, 15145–15148.
45 J. Zhao, J. Ren, G. Zhang, Z. Zhao, S. Liu, W. Zhang and L. Chen, *Chem.–Eur. J.*, 2021, **27**, 10781–10797.
46 Z. Fu, X. Wang, A. M. Gardner, X. Wang, S. Y. Chong, G. Neri, A. J. Cowan, L. Liu, X. Li, A. Vogel, R. Clowes, M. Bilton, L. Chen, R. S. Sprick and A. I. Cooper, *Chem. Sci.*, 2020, **11**, 543–550.
47 A. López-Magano, B. Ortín-Rubio, I. Imaz, D. Maspoch, J. Alemán and R. Mas-Ballesté, *ACS Catal.*, 2021, **11**, 12344–12354.
48 A. López-Magano, A. E. Platero-Prats, S. Cabrera, R. Mas-Ballesté and J. Alemán, *Appl. Catal., B*, 2020, **272**, 119027.
49 N. Rono, J. K. Kibet, B. S. Martincigh and V. O. Nyamori, *Crit. Rev. Solid State Mater. Sci.*, 2020, **46**, 189–217.
50 S. He, Q. Rong, H. Niu and Y. Cai, *Chem. Commun.*, 2017, **53**, 9636–9639.

51 Y. Yang, H. Niu, L. Xu, H. Zhang and Y. Cai, *Appl. Catal., B*, 2020, **269**, 118799.
52 Y. Zhu, D. Zhu, Q. Yan, C. Liu, K. Ling, Y. Liu, D. Lee, X. Wu, T. Senftle and R. Verduzco, *Chem. Sci.*, 2021, **12**, 16092–16099.
53 C. Singh, T. W. Kim, R. K. Yadav, J.-O. Baeg, V. Gole and A. P. Singh, *Appl. Surf. Sci.*, 2021, **544**, 148938.
54 Z. Almansaf, J. Hu, F. Zanca, H. R. Shahsavari, B. Kampmeyer, M. Tsuji, K. Maity, V. Lomonte, Y. Ha, P. Mastrorilli, S. Todisco, M. Benamara, R. Oktavian, A. Mirjafari, P. Z. Moghadam, A. R. Khosropour and H. Beyzavi, *ACS Appl. Mater. Interfaces*, 2021, **13**, 6349–6358.
55 Y. Chen, Y. Zhang and J. Huo, *J. Solid State Chem.*, 2022, **310**, 123047.
56 F. J. Uribe-Romo, J. R. Hunt, H. Furukawa, C. Klöck, M. O'Keeffe and O. M. Yaghi, *J. Am. Chem. Soc.*, 2009, **131**, 4570–4571.
57 E. Jin, M. Asada, Q. Xu, S. Dalapati, M. A. Addicoat, M. A. Brady, H. Xu, T. Nakamura, T. Heine, Q. Chen and D. Jiang, *Science*, 2017, **357**, 673–676.
58 H. Lyu, C. S. Diercks, C. Zhu and O. M. Yaghi, *J. Am. Chem. Soc.*, 2019, **141**, 6848–6852.
59 D. L. Pastoetter, S. Xu, M. Borrelli, M. Addicoat, B. P. Biswal, S. Paasch, A. Dianat, H. Thomas, R. Berger, S. Reineke, E. Brunner, G. Cuniberti, M. Richter and X. Feng, *Angew. Chem., Int. Ed.*, 2020, **59**, 23620–23625.
60 Y. Peng, W.-K. Wong, Z. Hu, Y. Cheng, D. Yuan, S.-A. Khan and D. Zhao, *Chem. Mater.*, 2016, **28**, 5095–5101.
61 E. L. Spitler, B. T. Koo, J. L. Novotney, J. W. Colson, F. J. Uribe-Romo, G. D. Gutierrez, P. Clancy and W. R. Dichtel, *J. Am. Chem. Soc.*, 2011, **133**, 19416–19421.
62 P. Kuhn, M. Antonietti and A. Thomas, *Angew. Chem., Int. Ed.*, 2008, **47**, 3450–3453.
63 X. Y. Guan, Y. C. Ma, H. Li, Y. Yusran, M. Xue, Q. R. Fang, Y. S. Yan, V. Valtchev and S. L. Qiu, *J. Am. Chem. Soc.*, 2018, **140**, 4494–4498.
64 L. K. Ritchie, A. Trewin, A. Reguera-Galan, T. Hasell and A. I. Cooper, *Microporous Mesoporous Mater.*, 2010, **132**, 132–136.
65 L. Chen, J. Du, W. Zhou, H. Shen, L. Tan, C. Zhou and L. Dong, *Chem.–Asian J.*, 2020, **15**, 3421–3427.
66 B. P. Biswal, S. Chandra, S. Kandambeth, B. Lukose, T. Heine and R. Banerjee, *J. Am. Chem. Soc.*, 2013, **135**, 5328–5331.
67 X. Zhang, Y. Yan, Q. Lu, B. He, S. Liu, M. Cai, Q. Ye and F. Zhou, *Tribol. Int.*, 2022, **176**, 107892.
68 S.-T. Yang, J. Kim, H.-Y. Cho, S. Kim and W.-S. Ahn, *RSC Adv.*, 2012, **2**, 10179–10181.
69 L. Stegbauer, S. Zech, G. Savasci, T. Banerjee, F. Podjaski, K. Schwinghammer, C. Ochsenfeld and B. V. Lotsch, *Adv. Energy Mater.*, 2018, **8**, 1703278.
70 S. Bi, Z.-A. Lan, S. Paasch, W. Zhang, Y. He, C. Zhang, F. Liu, D. Wu, X. Zhuang, E. Brunner, X. Wang and F. Zhang, *Adv. Funct. Mater.*, 2017, **27**, 1703146.
71 L. Wang, R. Lian, Y. Zhang, X. Ma, J. Huang, H. She, C. Liu and Q. Wang, *Appl. Catal., B*, 2022, **315**, 121568.
72 L. Li, W. Fang, P. Zhang, J. Bi, Y. He, J. Wang and W. Su, *J. Mater. Chem. A*, 2016, **4**, 12402–12406.
73 Y. Zheng, Y. Chen, L. Wang, M. Tan, Y. Xiao, B. Gao and B. Lin, *Sustainable Energy Fuels*, 2020, **4**, 3739–3746.
74 Y. Xing, L. Yin, Y. Zhao, Z. Du, H.-Q. Tan, X. Qin, W. Ho, T. Qiu and Y.-G. Li, *ACS Appl. Mater. Interfaces*, 2020, **12**, 51555–51562.
75 L. Stegbauer, K. Schwinghammer and B. V. Lotsch, *Chem. Sci.*, 2014, **5**, 2789–2793.
76 M. Luo, Q. Yang, K. Liu, H. Cao and H. Yan, *Chem. Commun.*, 2019, **55**, 5829–5832.
77 J. L. Sheng, H. Dong, X. B. Meng, H. L. Tang, Y. H. Yao, D. Q. Liu, L. L. Bai, F. M. Zhang, J. Z. Wei and X. J. Sun, *ChemCatChem*, 2019, **11**, 2313–2319.
78 B. P. Biswal, H. A. Vignolo-González, T. Banerjee, L. Grunenberg, G. Savasci, K. Gottschling, J. Nuss, C. Ochsenfeld and B. V. Lotsch, *J. Am. Chem. Soc.*, 2019, **141**, 11082–11092.
79 R. K. Yadav, A. Kumar, N.-J. Park, K.-J. Kong and J.-O. Baeg, *J. Mater. Chem. A*, 2016, **4**, 9413–9418.
80 Y. Fu, X. Zhu, L. Huang, X. Zhang, F. Zhang and W. Zhu, *Appl. Catal., B*, 2018, **239**, 46–51.
81 H. Zhong, Z. Hong, C. Yang, L. Li, Y. Xu, X. Wang and R. Wang, *ChemSusChem*, 2019, **12**, 4493–4499.
82 K. Lei, D. Wang, L. Ye, M. Kou, Y. Deng, Z. Ma, L. Wang and Y. Kong, *ChemSusChem*, 2020, **13**, 1725–1729.
83 Y. H. Kim, N. Kim, J. M. Seo, J. P. Jeon, H. J. Noh, D. H. Kweon, J. Ryu and J. B. Baek, *Chem. Mater.*, 2021, **33**, 8705–8711.
84 J. Li, P. Liu, H. Huang, Y. Li, Y. Tang, D. Mei and C. Zhong, *ACS Sustainable Chem. Eng.*, 2020, **8**, 5175–5183.
85 X. Song, Y. Wu, X. Zhang, X. Li, Z. Zhu, C. Ma, Y. Yan, P. Huo and G. Yang, *Chem. Eng. J.*, 2021, **408**, 127292.
86 N. Singh, D. Yadav, S. V. Mulay, J. Y. Kim, N. J. Park and J. O. Baeg, *ACS Appl. Mater. Interfaces*, 2021, **13**, 14122–14131.
87 L. Peng, S. Chang, Z. Liu, Y. Fu, R. Ma, X. Lu, F. Zhang, W. Zhu, L. Kong and M. Fan, *Catal. Sci. Technol.*, 2021, **11**, 1717–1724.
88 H. Huang, F. Li, Y. Zhang and Y. Chen, *J. Mater. Chem. A*, 2019, **7**, 5575–5582.
89 L. J. Wang, R. L. Wang, X. Zhang, J. L. Mu, Z. Y. Zhou and Z. M. Su, *ChemSusChem*, 2020, **13**, 2973–2980.
90 S. He, B. Yin, H. Niu and Y. Cai, *Appl. Catal., B*, 2018, **239**, 147–153.
91 S. Ma, Z. Li, J. Jia, Z. Zhang, H. Xia, H. Li, X. Chen, Y. Xu and X. Liu, *Chin. J. Catal.*, 2021, **42**, 2010–2019.
92 X. R. Chen, W. R. Cui, R. P. Liang, C. R. Zhang, R. H. Xu, W. Jiang and J. D. Qiu, *ACS Appl. Bio Mater.*, 2021, **4**, 6502–6511.
93 A. Jiménez-Almarza, A. López-Magano, R. Cano, B. Ortín-Rubio, D. Díaz-García, S. Gomez-Ruiz, I. Imaz, D. Maspoch, R. Mas-Ballesté and J. Alemán, *Mater. Today Chem.*, 2021, **22**, 100548.
94 T. Xia, Z. Wu, Y. Liang, W. Wang, Y. Li, Z. Sui, L. Shan, C. Li, R. Fan and Q. Chen, *Mater. Today Chem.*, 2022, **25**, 100962.

95 J. Pan, L. Guo, S. Zhang, N. Wang, S. Jin and B. Tan, *Chem.–Asian J.*, 2018, **13**, 1674–1677.
96 H. Xue, Z. Bi, J. Cheng, S. Xiong and Y. Wang, *Ind. Eng. Chem. Res.*, 2021, **60**, 8687–8695.
97 B. Zhang, F. Liu, C. Nie, Y. Hou and M. Tong, *J. Hazard. Mater.*, 2022, **435**, 128966.
98 Y. Yao, Y. Hu, H. Hu, L. Chen, M. Yu, M. Gao and S. Wang, *J. Colloid Interface Sci.*, 2019, **554**, 376–387.
99 F. Liu, Q. Dong, C. Nie, Z. Li, B. Zhang, P. Han, W. Yang and M. Tong, *Chem. Eng. J.*, 2022, **430**, 132833.
100 L. Niu, X. Zhao, F. Wu, H. Lv, Z. Tang, W. Liang, X. Wang and J. Giesy, *Chem. Eng. J.*, 2021, **414**, 128916.
101 H. Lv, X. Zhao, H. Niu, S. He, Z. Tang, F. Wu and J. P. Giesy, *J. Hazard. Mater.*, 2019, **369**, 494–502.
102 V. Saptal, D. B. Shinde, R. Banerjee and B. M. Bhanage, *Catal. Sci. Technol.*, 2016, **6**, 6152–6158.
103 Y. F. Zhi, P. P. Shao, X. Feng, H. Xia, Y. M. Zhang, Z. Shi, Y. Mu and X. M. Liu, *J. Mater. Chem. A*, 2018, **6**, 374–382.
104 P. Sarkar, A. Das, S. Ghosh and S. Manirul Islam, *ChemCatChem*, 2022, **14**, e202200186.
105 H. R. Liu, C. Z. Li, H. Li, Y. Q. Ren, J. Chen, J. T. Tang and Q. H. Yang, *ACS Appl. Mater. Interfaces*, 2020, **12**, 20354–20365.
106 P. Pachfule, A. Acharjya, J. Roeser, R. P. Sivasankaran, M.-Y. Ye, A. Brückner, J. Schmidt and A. Thomas, *Chem. Sci.*, 2019, **10**, 8316–8322.
107 H. Yang, Z. Lu, X. Fu, Q. Li, L. Xiao, Y. Zhao and L. Hou, *Eur. Polym. J.*, 2022, **173**, 111306.
108 R. Peng, Y. Luo, Q. Cui, H. Zhang and L. Li, *ACS Appl. Mater. Interfaces*, 2022, **14**, 49254–49263.
109 M. Liu, K. Jiang, X. Ding, S. Wang, C. Zhang, J. Liu, Z. Zhan, G. Cheng, B. Li, H. Chen, S. Jin and B. Tan, *Adv. Mater.*, 2019, **31**, 1807856.
110 X. Zhong, Z. Ren, Q. Ling and B. Hu, *Appl. Surf. Sci.*, 2022, **597**, 153621.
111 Q. Y. Wang, J. Liu, M. Cao, J. H. Hu, R. Pang, S. Wang, M. Asad, Y. L. Wei and S. Q. Zang, *Angew. Chem., Int. Ed.*, 2022, **61**, e202207130.
112 W. B. Chen, Z. F. Yang, Z. Xie, Y. S. Li, X. Yu, F. L. Lu and L. Chen, *J. Mater. Chem. A*, 2019, **7**, 998–1004.
113 F. Liu, Z. Ma, Y. Deng, M. Wang, P. Zhou, W. Liu, S. Guo, M. Tong and D. Ma, *Environ. Sci. Technol.*, 2021, **55**, 5371–5381.
114 S. Zhong, Y. Wang, S. Li, S. Wang, X. Que, L. Sheng, J. Peng, L. Zhao, L. Yuan and M. Zhai, *Sep. Purif. Technol.*, 2022, **294**, 121204.